



Heat exchangers fouling in phosphoric acid concentration

Ali Fguiri¹ · Rania Jradi¹ · Christophe Marvillet² · Mohamed Razak Jeday¹

Received: 22 January 2019 / Accepted: 16 March 2020 / Published online: 3 April 2020
© Springer-Verlag GmbH Germany, part of Springer Nature 2020

Abstract

Industrial heat exchanger fouling is generally defined as the accumulation and formation of undesired materials on the exchange surface. Experimental measurements of degree of fouling are both difficult and time consuming and often do not provide accurate results. However, the modeling of the thermal resistance of fouling can inform us on the evolution of this phenomenon. The present work aimed at studying fouling three types of heat exchangers, namely stainless-steel tubular and two graphite blocks from different suppliers (A and B), in an industrial phosphoric acid concentration unit belonging to the phosphoric acid production plant of the Tunisian Chemical Group (GCT) using the measurements of the operating parameters over a period of two years. The overall heat transfer coefficients and fouling resistances were evaluated at different times using the experimental data. Our results show that the resistance of fouling reach a maximal value ranging between $1.38 \cdot 10^{-4}$ and $2.55 \cdot 10^{-4} \text{ m}^2 \cdot \text{K} \cdot \text{W}^{-1}$ according to the type of the heat exchanger. Therefore, the experimental data of fouling resistances were compared with Kern and Seaton predictive model. Quantitative and qualitative agreement between measured and predicted fouling resistances is good with the coefficient of determination (R^2) varying between 0.97 and 0.98.

Nomenclature

C_p	Specific heat capacity, $\text{J} \cdot \text{K}^{-1} \cdot \text{kg}^{-1}$
F	Correction Factor
L_v	Latent heat of vaporisation, $\text{J} \cdot \text{kg}^{-1}$
\dot{m}	Mass flow rate, $\text{kg} \cdot \text{s}^{-1}$
n	Observation number
P	Pressure, bar
Q	Thermal power, W
R_f	Fouling resistance, $\text{m}^2 \cdot \text{K} \cdot \text{W}^{-1}$
A	Area, m^2
T	Temperature, K
t	Time, h
U	Overall heat transfer coefficient, $\text{W} \cdot \text{m}^{-2} \cdot \text{K}^{-1}$
\dot{v}	Volume flow rate, $\text{m}^3 \cdot \text{s}^{-1}$

Greek letters

Δ	Difference of greatness between two points
σ	Standard deviation
T	Time required to reach 63.2% of R_f^* , h

Subscripts

ac	Acid
cal	Calculated
cir	Circulation
dil	Diluted
ex	Exchange
exp	Experimental
in	Input
ml	Logarithmic average
out	Output
st	Steam
*	Asymptotic value

1 Introduction

The heat exchanger occupies an important and an indispensable place in all thermal systems, whether for industrial use (chemicals, petrochemicals, steel, food processing and energy production), for the automotive, aerospace, residential wether or tertiary building ... etc. [1]. In general, more than 90% of the thermal energy used in industrial processes passes at least once through a heat exchanger [1]. Industrial Heat exchanger main operating problems are due to fouling, corrosion, vibration and mechanical strength phenomena. Corrosion and fouling remain the most misunderstood phenomena in the industrial field. They impact sizing and aging of the equipment, and induce overheads (energy, shutdowns).

✉ Ali Fguiri
ali.fguiri@gmail.com

¹ Ecole Nationale d'ingénieurs de Gabes, Laboratoire de Recherche Procédés, Energétique, Environnement & Systèmes Electriques (PEESE), Avenue Omar Ibn El Khattab, 6029 Zrig Gabes, Tunisia

² Institut Français de Froid Industriel, Laboratoire CMGPCE, CNAM-Paris, 292 Rue, 75003 Paris, Saint-Martin, France

Fouling is defined as accumulation of unwanted or undesirable deposits on heat transfer surface. In general, it refers to the collection and growth of detrimental materials on heat transfer surface, which significantly declines its thermal performance. Fouling process incorporates various heat, mass and energy transfer phenomenon involved with heat exchanger operations [2]. Several categories of deposits have been listed. The type of deposit is different from one industry to another. Many authors [3, 4] have proposed a classification of deposits in 6 types based on the main physical and chemical mechanisms at the origin of their formation. According to this classification, the types of fouling may be particulate fouling, crystallization (precipitation fouling), chemical reaction fouling, corrosion fouling, biological fouling, or solidification (freezing fouling).

In order to make the decision to clean or repair the heat exchanger, it is necessary to monitor the level of fouling on the exchange surface. Modeling the fouling resistance according to the operating parameters of the exchanger, helps the industrialist to follow the fouling and to proceed with the cleaning of the exchanger. Several authors [5, 6] have studied this phenomenon of fouling based on the modeling of the thermal resistance of fouling. Mariusz et al. [7] used the heat exchanger model with improved correlation of the heat transfer coefficient in order to estimate the thermal fouling resistance. Mohammad Awais et al. [8] presented a review study which would be exceedingly useful for designers to design heat exchanger with higher overall efficiency under the influence of fouling. Fguiiri et al. [9] carried out an experimental study on three types of exchangers and showed that the global exchange coefficient reached its minimum value when the exchanger was in maximum fouling. The prediction and modeling of the fouling resistance of a plate heat exchanger using the neuron network method [10, 11] was carried out by Weber et al. [12] based on experimental data. The results obtained where in good agreement with the model of Kern and Seaton [13]. Behbahani et al. [14] have shown from experiments carried out in a phosphoric acid production unit that the fouling resistance of the exchanger depends on flow velocities, surface temperatures and concentrations, this study helps industrial to determine the mechanisms which control the deposition process.

In this work, we present an analysis of the resistance of fouling heat exchanger (phosphoric acid / vapor) in an industrial phosphoric acid concentration unit belonging to the phosphoric acid production plant of the Tunisian Chemical Group (GCT). Three types of exchanger are used to see their effect on fouling. The input-output temperature measurements of the phosphoric acid and steam are measured to calculate the thermal fouling resistance. Experimental fouling kinetics are compared with the Kern and Seaton model in order to identify the maximum fouling resistance and assist the industrialist in the cleaning decision.

1.1 Description of the industrial unit

Generally, in the phosphoric acid production industry, the concentration of phosphoric acid from 28% P_2O_5 to 54% P_2O_5 is carried out in a closed loop forced-circulation evaporator, operating in vacuum Tanks to a barometric condenser. The concentration system used is constituted by a tubular heat exchanger made of stainless steel [15] or graphite blocks (A) [16], a circulating pump (B), a boiler or expansion chamber (C), a barometric condenser (D) and a basket filter (E) [13] (Fig. 1). The graphite blocks heat exchangers used in this work were provided by two different manufacturers (labeled provider (A) and (B)).

The addition of the dilute phosphoric acid (1) takes place at the basket filter where it mixes with the circulating phosphoric acid (2) in order to protect the pump from abrasion and limit the fouling of the exchanger. This makes it possible to minimize the frequency of stopping for washing. The circulation pump aspirates the blend formed and sends it to the inlet of the heat exchanger at a temperature of about 70 °C to raise it to about 80 °C. The steam inlet (3) undergoes a condensation at the heat exchanger at a temperature of 120 °C. The condensate outlet (4) is sent to a storage tank before being sent back to the utility station. The superheated mixture of phosphoric acid (5) leaving the exchanger then passes into the boiler where a quantity of water evaporates (6) and the concentrated acid (7) is produced by overflowing in a piping system inside the boiler and the rest is recycled. The condenser also ensures incurring uncondensables coming out of the boiler (8) by the effect of a hydro-ejector valuing the relaxation of pressurized water flow (9). At the foot of the barometric guard, the sea water is recovered in a barometric seal before being released into the sea.

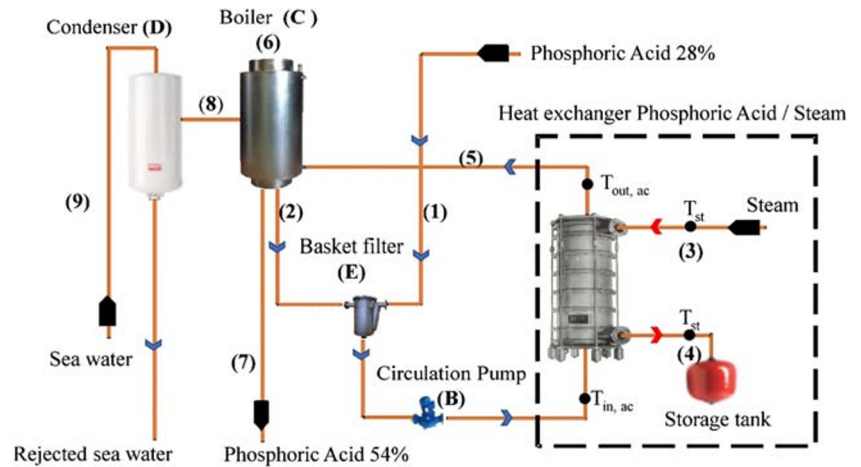
The washing operation of concentration loop is carried out using sea water to guarantee that the heat exchanger is totally free of fouling at the beginning of a new run. This operation consists of emptying the concentration loop of the phosphoric acid, filling it with sea water, circulating the sea water in the loop for a while, emptying the sea water and filling it again with phosphoric acid.

The main characteristics of the exchangers used for the concentration of phosphoric acid are given in Table 1:

1.1.1 Thermal modeling

For the three studied exchangers, the flow of the two fluids (phosphoric acid and steam) is at counter current. Values of the thermo-physical properties of the fluids were considered constant and the thermal losses were neglected. A procedure was set up in the concentration loop in order to control the thermal and hydraulic performances of the exchanger through the measurement of temperature, steam pressure, suction and discharge pressure of the pump and flow rate of dilute

Fig. 1 Phosphoric-acid concentration unit



phosphoric acid. The flow rate of circulating phosphoric acid was calculated from the characteristic curve of the pump [17].

Measurements of three temperatures over time are made using three thermocouples type Pt100 class A, the uncertainties on the temperature is ± 0.3 °C. The density of the phosphoric acid was measured with a Densimeter DMA35 with the uncertainty of $\pm 0.05\%$. The pressure was measured using a Diaphragm pressure gauge with the uncertainty of $\pm 1.6\%$. Finally, the volume flow rate of phosphoric acid was measured using a flow meter and this with the uncertainty of 2%.

The data is acquired by a computer system present in the control room. The data was collected for the 3 studied exchangers over a 2-year operation period.

The fouling resistance (R_f) is calculated using the following expression [18]:

$$R_f(t) = \frac{1}{U(t)} - \frac{1}{U(t=0)} \tag{1}$$

where $U(t)$ is the overall heat transfer coefficient characterizing the heat exchanger and $U(t=0)$ is the clean heat transfer coefficient.

Before starting the calculation of the global exchange coefficient, we will determine the volume flow rate of phosphoric acid using the characteristic curve of the circulation pump presented by the equation [17]:

$$\dot{v}_{ac} = f(HMT) \tag{2}$$

Where HMT is the manometric head of the pump expressed as follows:

Table 1 The three studied exchangers

Type of exchanger	Main characteristics	
Stainless-steel tubular heat exchanger (Figure 2)	Number of tubes	395
	Tube diameter (mm)	23
	Exchange surface (m ²)	189.5
	Type of steel dye	316
Graphite blocks heat exchanger (provider A) (Figure 3)	Number of blocks	11
	Diameter of acid-side duct (mm)	16
	Diameter of steam-side duct (mm)	15
	Exchange surface (m ²)	249.5
	Number of acid-side ducts	868
	Number of steam-side ducts	483
Graphite blocks heat exchanger (provider B) (Figure 3)	Type of graphite	Graphilor®3
	Number of blocks	11
	Diameter of acid-side duct (mm)	16
	Diameter of steam-side duct (mm)	15
	Exchange surface (m ²)	249.5
	Number of acid-side ducts	868
Number of steam-side ducts	437	
	Type of graphite	DIABON

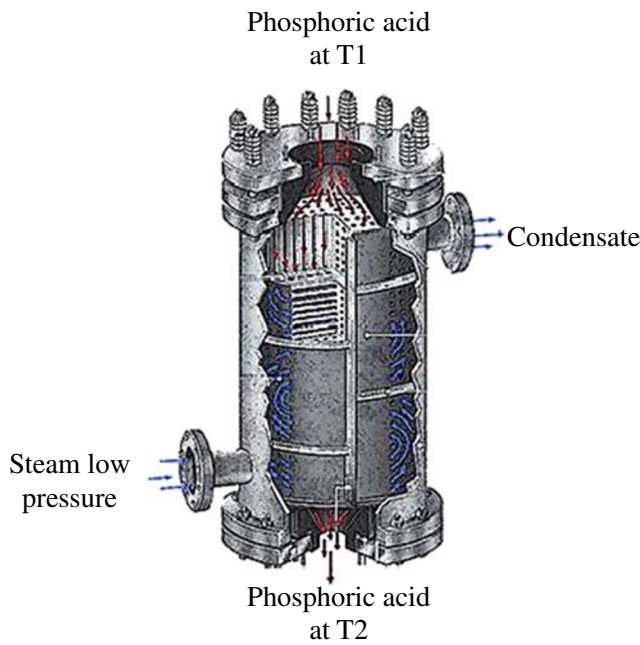


Fig. 2. Photograph of the stainless-steel-tubular heat exchanger [15]

$$HMT = \frac{P_s - P_d}{\rho_{ac} \cdot g} \tag{3}$$

Where P_s and P_d are the suction and discharge pressure of the pump, respectively, ρ_{ac} is the density of phosphoric acid, and g is the gravity acceleration ($g = 9.81 \text{ m s}^{-2}$).

The overall heat transfer coefficient $U(t)$ is evaluated from industrial measurements of operating data and using the equations of energy balance (4), (5) and (6). The initial value of the overall heat transfer coefficient $U(t=0)$ at the beginning of every cycle is considered as the value of the clean heat transfer coefficient.

$$Q = \dot{m}_{st} \cdot L_v \tag{4}$$

$$Q = \rho_{ac} \cdot \dot{v}_{ac} \cdot C_{pac} \cdot \Delta T_{ac} = \dot{m}_{ac,cir} \cdot C_{pac} \cdot (T_{out,ac} - T_{in,ac}) \tag{5}$$

$$Q = F \cdot U(t) \cdot A \cdot \Delta T_m \tag{6}$$

$$\Delta T_m = \frac{(T_{st} - T_{in,ac}) - (T_{st} - T_{out,ac})}{\ln\left(\frac{(T_{st} - T_{in,ac})}{(T_{st} - T_{out,ac})}\right)} \tag{7}$$

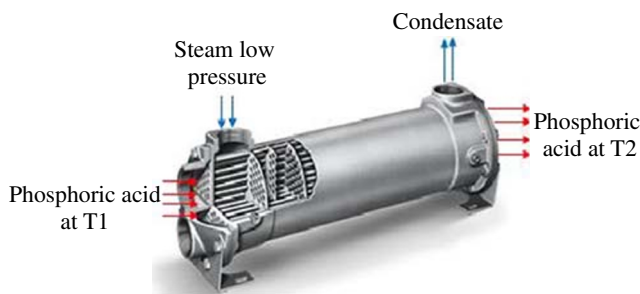


Fig. 3. Photograph of the graphite blocks heat exchanger [16]

Where Q is the thermal power (W), A is the exchange area (m^2), $\dot{m}_{ac,cir}$ and \dot{m}_{st} are respectively the mass flow rate of circulating phosphoric acid which is the cold fluid ($\text{kg} \cdot \text{s}^{-1}$) and the mass flow rate of steam which is the hot fluid ($\text{kg} \cdot \text{s}^{-1}$), ΔT_m is the logarithmic average temperature difference (K), C_{pac} is the specific heat of phosphoric acid equal to $2135 \text{ J} \cdot \text{kg}^{-1} \cdot \text{K}^{-1}$, and F is the corrective coefficient of the average logarithmic temperature difference.

1.2 Thermal modeling of fouling resistance

From a literature review [13, 19–21], we note that the model of Kern and Seaton is the model most used to describe the evolution of the thermal resistance of fouling during the operation of the process. The modeling stemming from this model is based on the hypothesis that two processes act in a simultaneous way. The first process is the one of the particles deposit characterized by a deposit flow ϕ_d which is constant if the concentration is it also. The second process is the one of the retraining of particles characterized by a retraining flow ϕ_r dependent on the mass of particles (m_p) deposited. The particulate balance of the deposit is expressed according to the following equation:

$$\frac{dm_p}{dt} = \Phi_d - \Phi_r \tag{8}$$

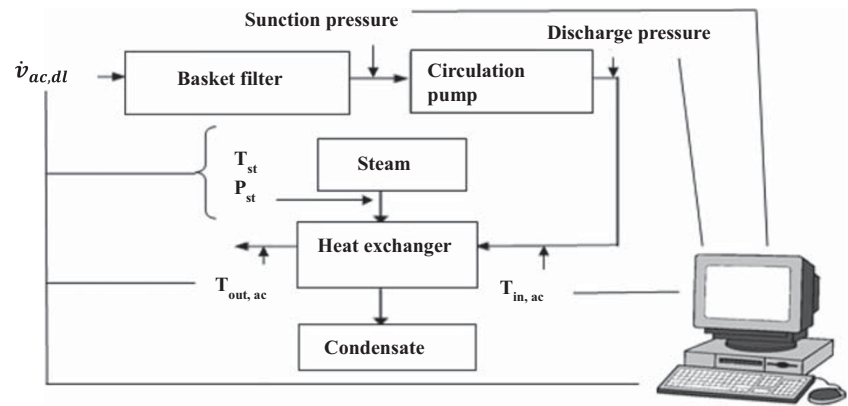
The deposition process is designed as the serialization of particle transport and adhesion mechanisms. Several assumption are made such as: the consideration of a single type of fouling; deposit homogeneity, not taking into account the deposit initiation phase and the surface state; and the properties and thermo-physical characteristics of the fluid and the deposit are constant.

The particle wall transport phase controls the deposition process while the shear stress controls the retraining phase of the particles. Thus, considering the proportionality of ϕ_d as a function of the deposited mass of particles, we can write the following equations:

Table 2 Uncertainties of direct and indirect measured values

Items	Parameters	Uncertainties
Direct measured values	Temperature	$\pm 0.3 \text{ }^\circ\text{C}$
	Density	$\pm 0.05\%$
	Pressure	$\pm 1.6\%$
	volume flow rate	$\pm 2\%$
Indirect measured values	Q	3.6%
	U	4.6%
	R_f	6.5%

Fig. 4 Acquisition of data



$$\phi_d = K_p^*(C_b - C_w) \tag{9}$$

$$\phi_r = C_1 * \tau_w * m_p \tag{10}$$

Where K_p is the transport coefficient; C_b is the concentration of particles within the fluid; C_w is the particle concentration at the wall; C_1 is a dimensional constant; τ_w is the shear stress exerted by the fluid on the deposit.

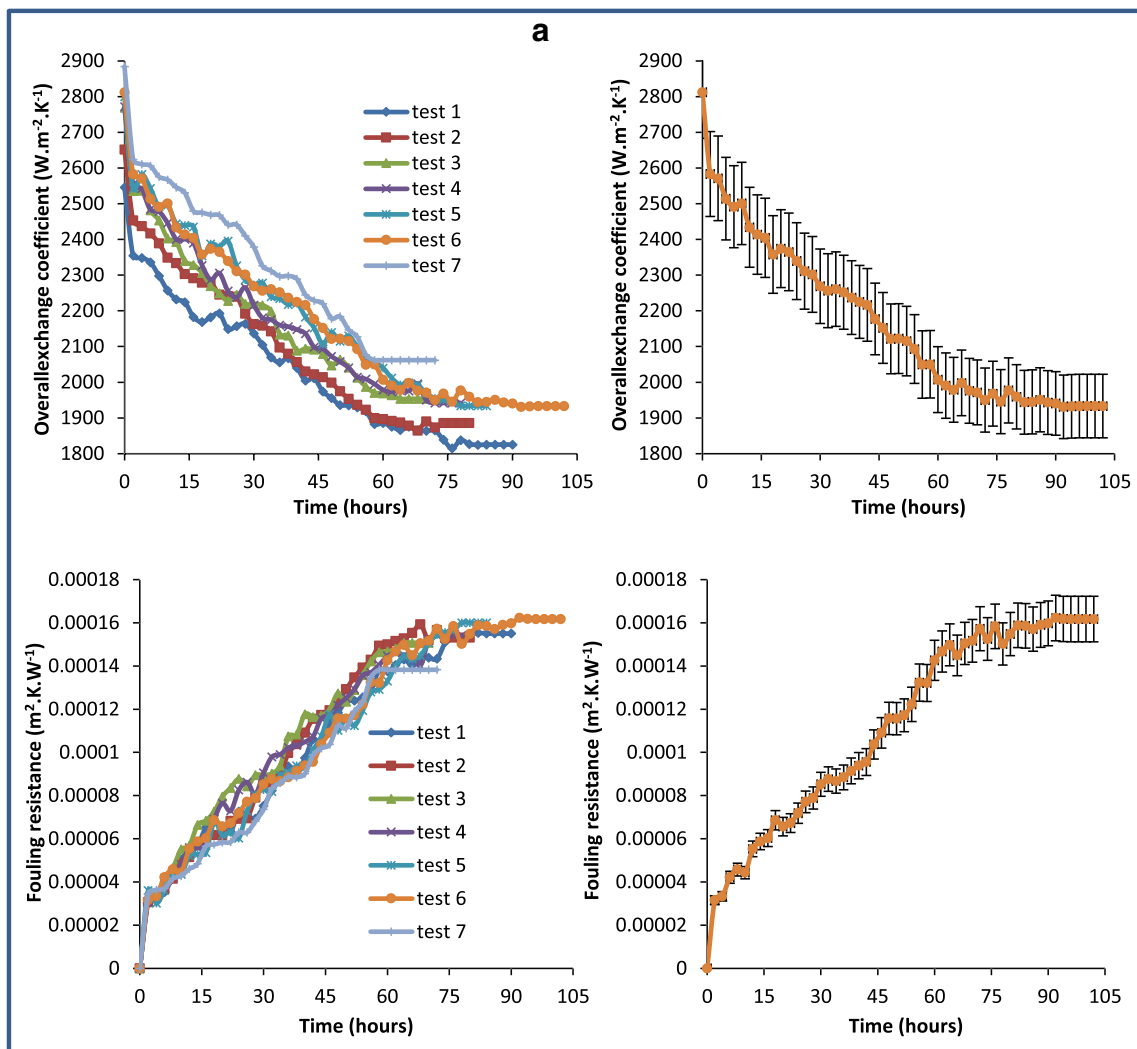


Fig. 5 (a): Variation of the overall exchange coefficient and the fouling resistance as a function of time for Stainless-steel tubular heat exchanger. b: Variation of the overall exchange coefficient and the fouling resistance

as a function of time for Graphite blocks heat exchanger (provider A). c: Variation of the overall exchange coefficient and the fouling resistance as a function of time for Graphite blocks heat exchanger (provider B).

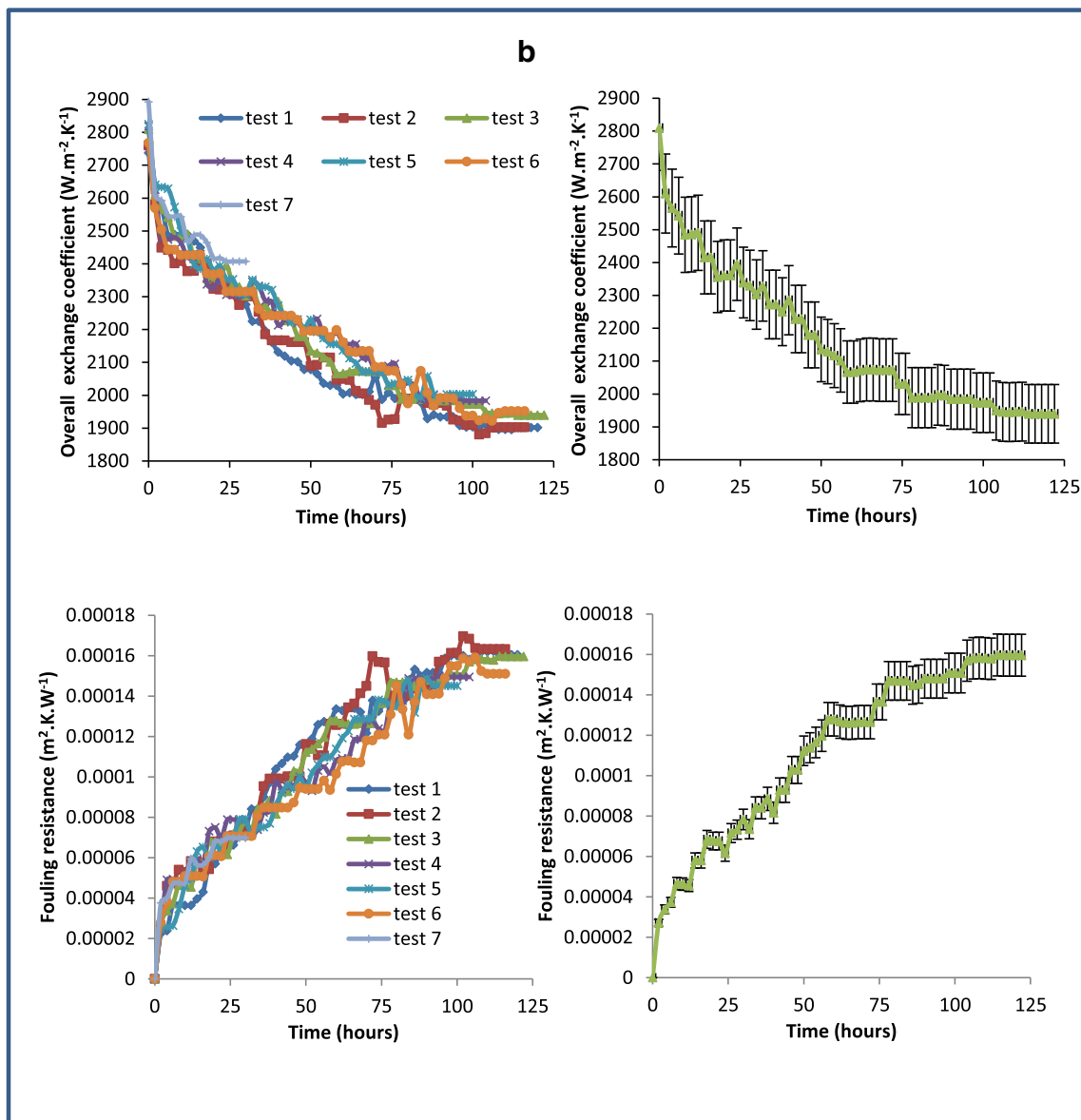


Fig. 5 (continued)

Using eqs. (9) and (10), eq. (8) becomes:

$$\frac{dm_p}{dt} = K_p * (C_b - C_w) - C_1 * \tau_w * m_p \tag{11}$$

The solution of eq. (11) is thus:

$$m_p = \frac{K_p * (C_b - C_w)}{C_1 * \tau_w} * [1 - \exp(-C_1 * \tau_w * t)] \tag{12}$$

Assuming that $\tau = \frac{1}{C_1 * \tau_w}$ and $m_p^* = \frac{K_p * (C_b - C_w)}{C_1 * \tau_w}$.

We can thus express the equation as follows:

$$m_p = m_p^* * \left[1 - \exp\left(-\frac{t}{\tau}\right) \right] \tag{13}$$

Considering that the initial fouling flow is equal to the deposition flow and that the thermo physical properties of the deposit (conductivity and density) are constant, it is thus possible to express eq. (13) in the form of a thermal fouling resistance:

$$Rf(t) = Rf^* * \left(1 - e^{-t/\tau} \right). \tag{14}$$

We quantify the model accuracy from the following indicators: the standard deviation σ of the relative error ε , the mean relative error as well as the determination coefficient R^2 (the square of the Pearson correlation coefficient) according to the following definitions [22]:

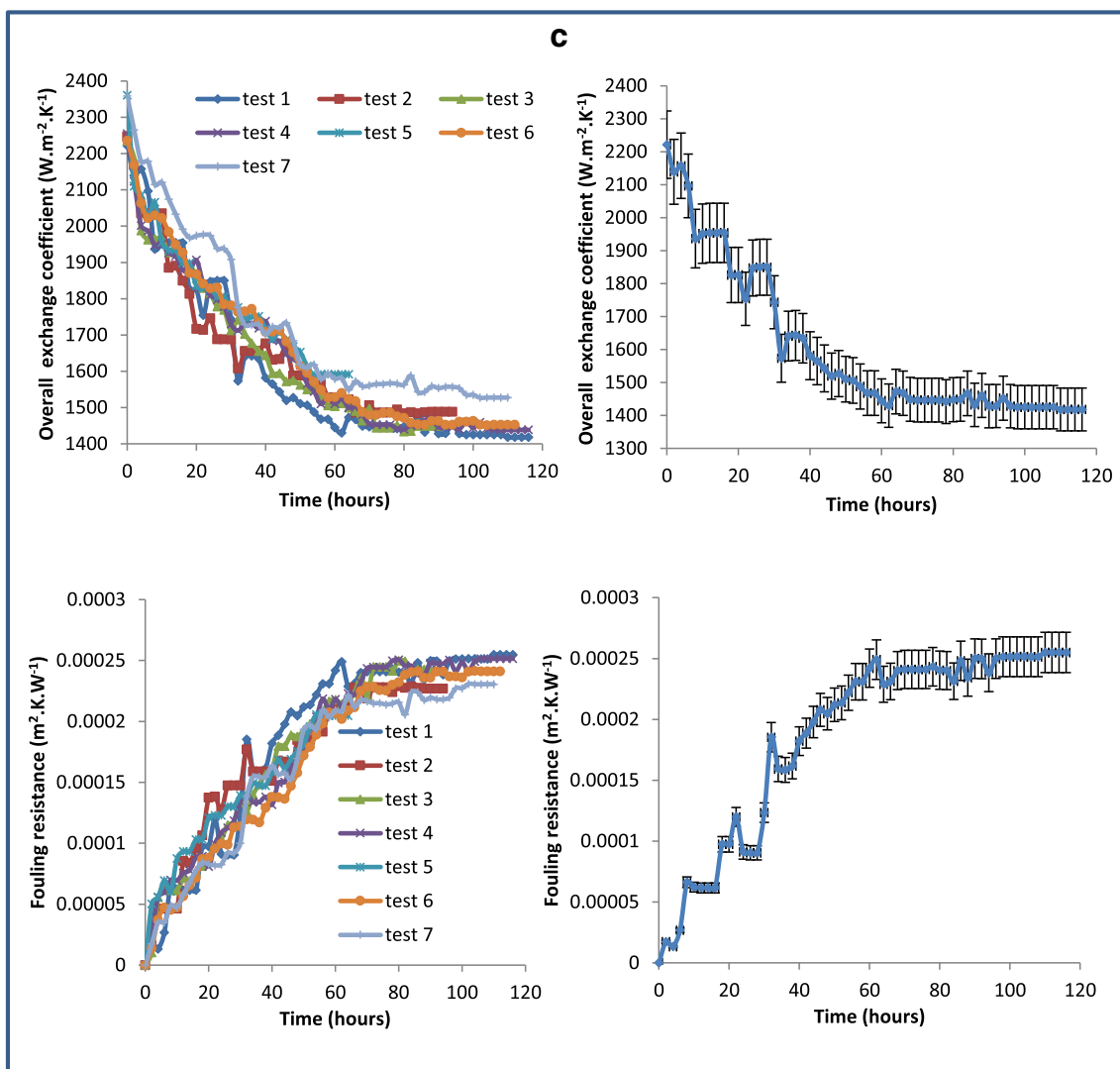


Fig. 5 (continued)

$$\varepsilon = \frac{100}{N} \sum_{i=1}^N \frac{(Rf_i^{exp} - Rf_i^{cal})}{Rf_i^{exp}} \quad (15)$$

$$\sigma = \sqrt{\frac{\sum_{i=1}^N (Rf_i^{exp} - \overline{\Delta Rf})^2}{N-1}} \quad (16)$$

$$R^2 = \frac{\sum_{i=1}^N (Rf_i^{exp} - \overline{\Delta Rf})^2 - \sum_{i=1}^N (Rf_i^{exp} - \Delta Rf_i^{cal})^2}{\sum_{i=1}^N (Rf_i^{exp} - \overline{\Delta Rf})^2} \quad (17)$$

Where Rf represent the fouling resistance. Rf^{exp} and Rf^{cal} respectively represent experimental and predicted fouling resistance. ΔRf is the average value of the experimental fouling resistance.

1.3 Uncertainty analysis

The uncertainty analysis on the measured data is carried out using the second power transfer method [23]. We assume that the relation between the variable (b) and independent variables a_1, a_2, \dots, a_n can be expressed as $b = f(a_1, a_2, \dots, a_n)$, and the uncertainties of each variable a_i is δa_i . The uncertainty of variable b is:

$$\delta b = \sqrt{\sum_{i=1}^n \left(\frac{\partial b}{\partial a_i} \delta a_i \right)^2} \quad (18)$$

The relative uncertainty of heat exchange (Q) is:

$$\frac{\delta Q}{Q} = \sqrt{\left(\frac{\delta \rho_{ac}}{\rho_{ac}} \right)^2 + \left(\frac{\delta v_{ac}}{v_{ac}} \right)^2 + \left(\frac{\delta \Delta T_{ac}}{\Delta T_{ac}} \right)^2} \quad (19)$$

Thus the relative uncertainty of heat transfer coefficient is:

$$\frac{\delta U}{U} = \sqrt{\left(\frac{\delta Q}{Q}\right)^2 + \left(\frac{\delta \Delta T_m}{\Delta T_m}\right)^2} \quad (20)$$

Similarly, the relative uncertainty of the fouling resistance is:

$$\frac{\delta R_f}{R_f} = \sqrt{\left(\frac{\delta U}{U}\right)^2 + \left(\frac{\delta U_0}{U_0}\right)^2} \quad (21)$$

Table 2 shows the uncertainties of the direct and indirect measured results. It can be seen the relative uncertainties of heat exchange, Q , overall heat exchange coefficient U and fouling resistance R_f are within 3.6%, 4.6% and 6.5% respectively.

2 Results and discussion

From the operating data collected on site and eqs. (4), (5) and (6), we evaluated the variation of the fouling resistance as a function of time for each type of exchanger. Fig. 5(a, b and c) shows the temporal evolution of the overall heat transfer coefficient $U(t)$ and the fouling resistance $R_f(t)$ for the three heat exchanger types. In order to avoid any confusion on experimental data, we presented for each exchanger a single cycle which contains the error bar.

We notice that the fouling resistance has an asymptotic pace which is in agreement with the most widely used model in the study of fouling, i.e. Kern and Seaton model, despite the presence of deviation for some experimental points, which may be imputed to the difference of operating data withdrawal time. It reaches a maximum value, ranging from $1.38 \cdot 10^{-4}$ to $2.55 \cdot 10^{-4} \text{ m}^2 \cdot \text{K} \cdot \text{W}^{-1}$ depending on the type of exchanger studied. This can be attributed to the growth phase of the crystal lattice which causes a degradation in the efficiency of the exchanger. During the remainder of the cycle, the fouling resistance remains constant: this is the removal phase during which the thickness of the fouling layer remains invariable as well as the formation and removal rates become equal. Furthermore, fouling resistance increases over time, which leads to a decrease in the flow of heat exchanged between the phosphoric acid and the steam, and subsequently the

decrease in the overall heat transfer coefficient. We also notice that for each operating cycle, the fouling resistance $R_f(t)$ converges to a maximum value that can be reduced to zero between operational runs following the cleaning operation. For example, the maximum values of the fouling resistance for 7 operating cycles of the stainless-steel tubular heat exchanger varied from $1.38 \cdot 10^{-4}$ to $1.61 \cdot 10^{-4} \text{ m}^2 \cdot \text{K} \cdot \text{W}^{-1}$. It should be noted that the appearance of the fouling initiation phase for the three studied types of exchangers is difficult to detect. This is probably related to the rapid evolution of this phenomenon associated in particular with the characteristics of the treated phosphoric acid.

As can be seen from Fig. 5, the time required to reach a fouling deposit is 70 h for the stainless-steel tubular heat exchanger and the graphite blocks heat exchanger (provider (B)) compared with 90 h for the graphite blocks heat exchanger (provider (A)). As of that moment, the asymptotic zone begins and the fouling thickness does not vary any more overtime. Furthermore, we notice a significant difference between the asymptotic values of the fouling resistance equal to $1.48 \cdot 10^{-4}$, $1.46 \cdot 10^{-4}$ and $2.24 \cdot 10^{-4} \text{ m}^2 \cdot \text{K} \cdot \text{W}^{-1}$ for stainless steel tubular, graphite blocks (provider (A)) and graphite blocks (provider (B)) exchangers, respectively.

For the seven cycles presented in Fig. 5a, b and c, all the curves have asymptotic appearance for the resistance of fouling. There is a small difference for the maximum fouling resistance; which is the immediate result of both a bad cleaning and the wrong time chosen by the industrialist to clean the exchanger. For this reason, we have chosen to model this fouling phenomenon in order to correctly detect the cleaning time.

The model of Kern and Seaton gives satisfying results provided that the asymptotic value of the fouling resistance (R_f^*) as well as the time constant (τ) which condition the accuracy of the model are well evaluated. Comparing these experimental results with the Kern model amounts to identifying two parameters which are R_f^* and τ and replacing them in the expression of the fouling resistance (eq. (14)). The method used is the Levenberg-Marquardt [24] method which consists in minimizing the quadratic sum of the difference between experimental measurement and Kern model according to the following expression:

$$S(R_f^*, \tau) = \sum_{i=1}^n (R_f(t_i) - R_{fexp}(t_i))^2 \quad (23)$$

Table 3 Values of the asymptotic fouling resistance, the time constant and the statistical accuracy indices for the studied exchanger types

Type of exchanger	$R_f^* (\text{m}^2 \cdot \text{K} \cdot \text{W}^{-1})$	τ (h)	R^2	σ	$\epsilon(\%)$
Stainless-steel tubular	$1.72 \cdot 10^{-4}$	40.32	0.9757	$4.57 \cdot 10^{-5}$	-4.01
Graphite blocks					
Provider (A)	$1.51 \cdot 10^{-4}$	42.01	0.9742	$4.02 \cdot 10^{-5}$	-4.68
Provider (B)	$2.59 \cdot 10^{-4}$	39.68	0.9856	$6.88 \cdot 10^{-5}$	-1.31

Fig. 6 **a** Kinetics of fouling for Stainless-steel tubular heat exchanger. **b**: Kinetics of fouling for Graphite blocks heat exchanger (provider A). **c**: Kinetics of fouling for Graphite blocks heat exchanger (provider B)

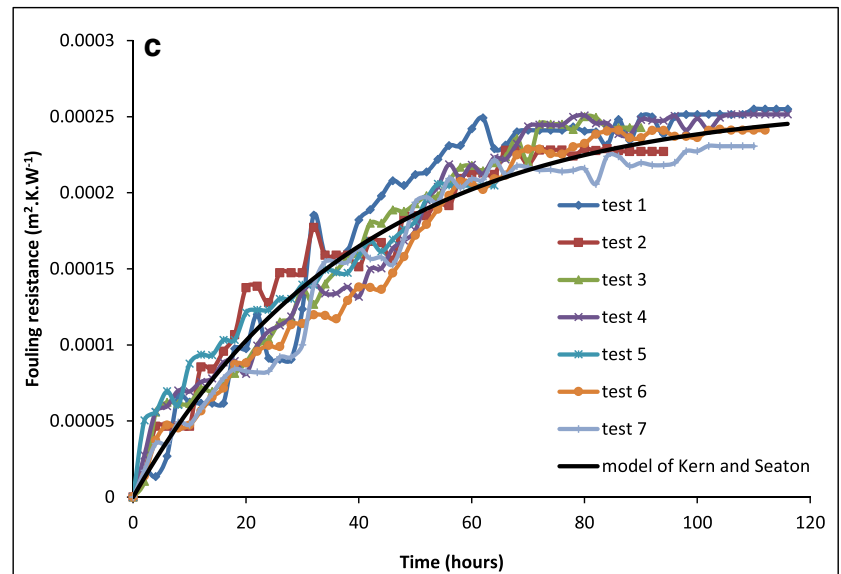
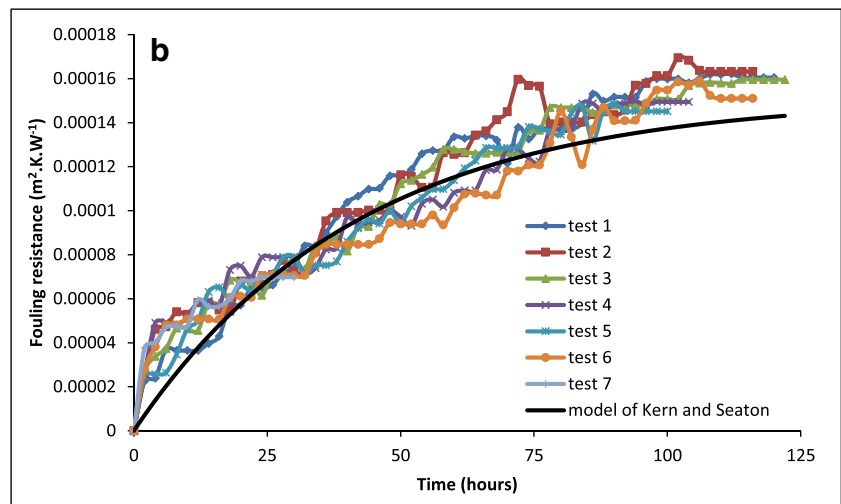
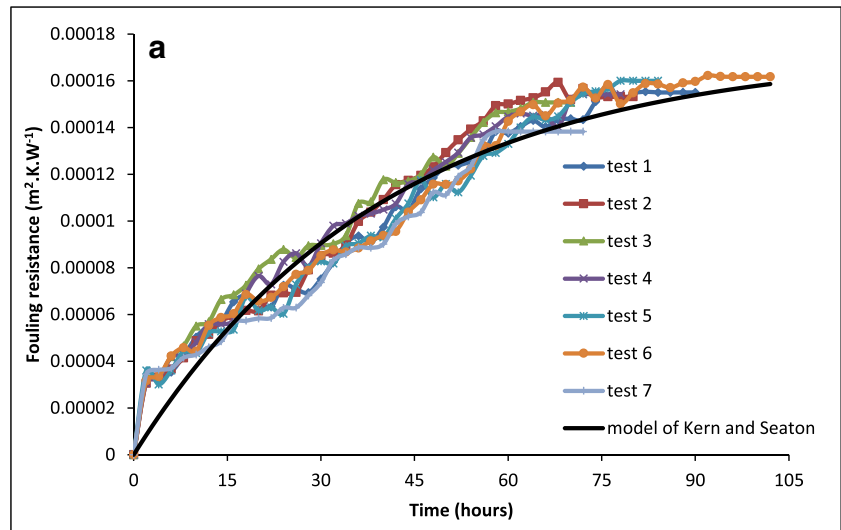
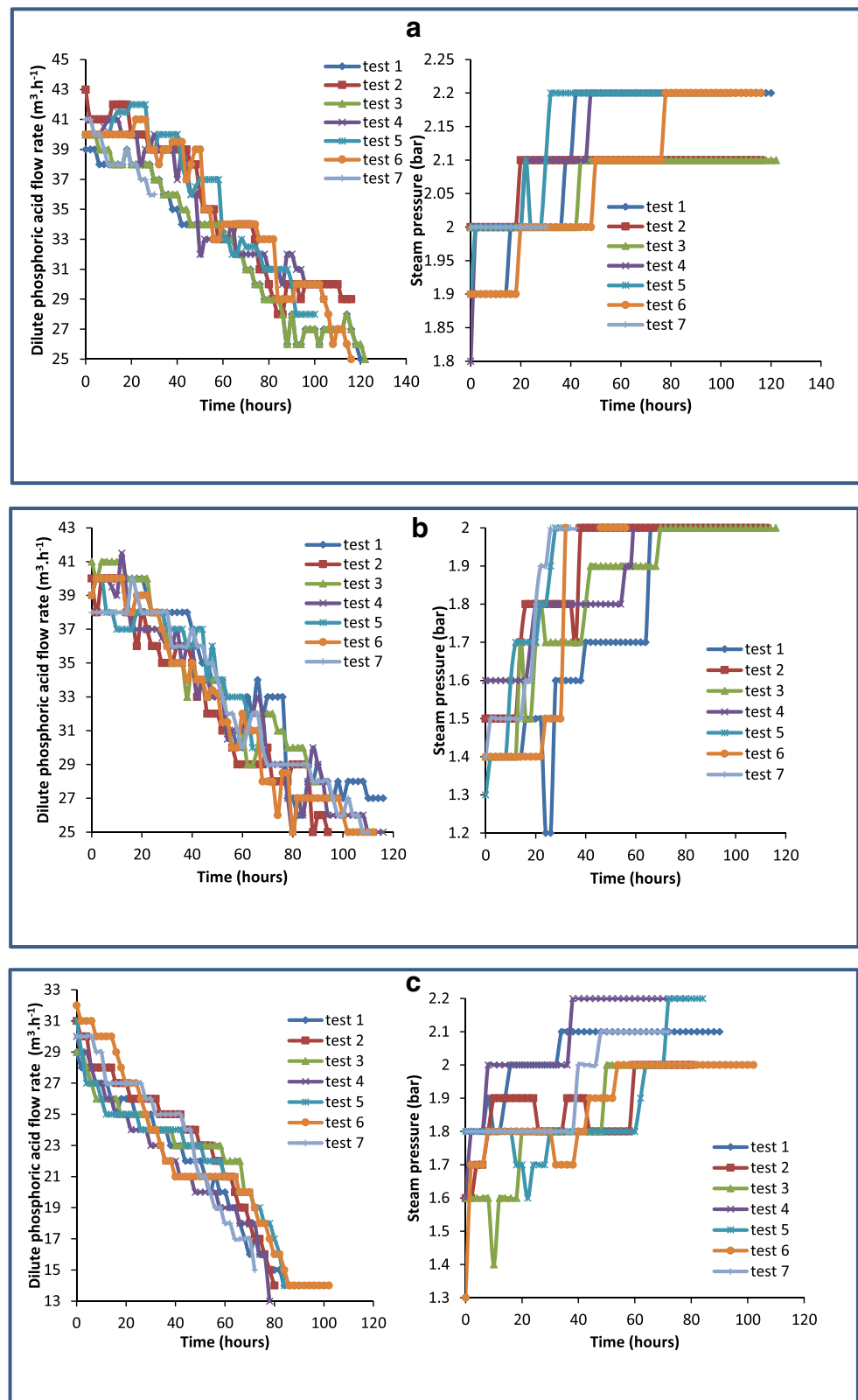


Fig. 7. (a) Variation of dilute phosphoric acid flow rate and steam pressure as a function of time for Stainless-steel tubular heat exchanger. **b:** Variation of dilute phosphoric acid flow rate and steam pressure as a function of time for Graphite blocks heat exchanger (provider A). **c:** Variation of dilute phosphoric acid flow rate and steam pressure as a function of time for Graphite blocks heat exchanger (provider B).



Where S is the quadratic sum, $R_f(t_i)$ is the fouling resistance at time t_i according to the model of Kern and Seaton, and $R_{fexp}(t_i)$ is the fouling resistance derived from measurements of the operating parameters of the exchanger at the same time t_i .

Table 3 presents the identification results of two parameters R_f^* and τ for the three types of heat exchangers. The value of the determination coefficient which is close to 1 shows a good agreement between the Kern and Seaton model, and the

experimental data. The values of the relative error ε (%) are relatively low with a maximum value equal to -4.68% for the graphite blocks heat exchanger (supplier (A)) and very low values of the standard deviation σ which are higher to 4.02×10^{-5} .

Figure 6 (a, b and c) illustrates the consistency in variation of the fouling resistance over time obtained from both measurement and the Kern and Seaton model. Figures 6, b and c show the good superposition of the fouling resistance obtained from the operational data measurements and the Kern and Seaton model by using the two parameters identifying Rf^* and τ with a maximum relative error for the three types of exchangers of 4.68% . Fig. 7 shows the evolution of the dilute phosphoric acid flow rate and the steam pressure over time for the three types of exchangers as a function of the fouling phenomenon.

It can be noticed that, from Fig. 5 and 7 (a, b and c), when the deposit appears in the exchanger, for $t = 70$ h for the stainless-steel tubular heat exchanger and the graphite blocks heat exchanger (provider (B)) and $t = 90$ h for the graphite blocks heat exchanger (provider (A)), the dilute phosphoric acid flow decreases by $13 \text{ m}^3 \cdot \text{h}^{-1}$, while the steam pressure increases by 0.5 bar. Those two quantities are the main indicators used by industrialists to monitor and control the fouling phenomenon in heat exchangers. Limit values of acid flow and steam pressure to trigger the heat exchanger cleaning process are respectively $15 \text{ m}^3 \cdot \text{h}^{-1}$ and 1 bar.

3 Conclusion

A theoretical and experimental study of industrial fouling heat exchangers has been carried out successfully. Three types of Phosphoric Acid / Steam heat exchangers (stainless steel tubular, graphite blocks from provider (A) and provider (B)) of a phosphoric acid concentration unit belonging to the phosphoric acid production plant of the Tunisian Chemical Group (GCT) were used in order to see the effect of type heat exchanger on fouling. An experimental study was carried out based on the transient measurements of the operating parameters for each type of heat exchanger such as $T_{ac, in}$, $T_{ac, out}$, T_{st} and mac . From these data measured on industrial sites, we calculated the thermal resistance of experimental fouling. The result of the experimental study showed us that the graphical representation of the thermal resistance of fouling as a function of time is asymptotic. For this reason, we have chosen the Kern and Seaton model for the theoretical study. The modeling of the Kern and Seaton fouling resistance was carried out using the Levenberg Marquardt method to identify the two parameters R^* and τ . Replacing these two parameters in the expression of the model of Kern and Seaton, we have noticed that the experimental results obtained from industrial data are in agreement with the evaluated data obtained using

the model of Kern and Seaton. The perspective of this work is to develop the study of fouling resistance, first by increasing the number of measurements and reducing the time scale and second by introducing a method of data analysis to model the fouling resistance.

References

1. Demasles H, Mercier P, Tochon P, Thonon B (2007) Guide de l'encrassement des échangeurs de chaleur, Editions GRETH. <https://greth.fr/guide-de-lencrassement/>
2. Harche R, Mouheb A, Absi R (2016) The fouling in tubular heat exchanger of Algiers refinery, heat and mass transfer 52:947–956. <https://doi.org/10.1007/s00231-015-1609-0>
3. Awad MM (2011) Fouling of heat transfer surface, Intech Open. <https://doi.org/10.5772/13696> <https://www.intechopen.com/books/heat-transfer-theoretical-analysis-experimental-investigations-and-industrial-systems/fouling-of-heat-transfer-surfaces>
4. Shen C, Wang Y, Tang Z, Yang Y, Huang Y, Wang X (2019) Experimental study on the interaction between particulate fouling and precipitation fouling in the fouling process on heat transfer tubes. Int J Heat Mass Transf 138:1238–1250
5. Zhiming Xu, Yu Zhao, Zhimin Han, Jingtao Wang, numerical simulation of calcium sulfate (CaSO_4) fouling in the plate heat exchanger, Heat Mass Transf, 54 (2018) 1867–1877
6. Song J, Liu Z, Ma Z, Zhang J (2017) Experimental investigation of convective heat transfer from sewage in heat exchange pipes and the construction of a fouling resistance-based mathematical model. Energy Buildings 150:412–420
7. Markowski M, Trzcinski P (2019) On-line control of the heat exchanger network under fouling constraints. Energy 185:521–526
8. Awais M, Bhuiyan AA (2019) Recent advancements in impedance of fouling resistance and particulate depositions in heat exchangers. Int J Heat Mass Transf 141:580–603
9. Jradi R, Fguiri A, Marvillet C, Jeday MR (2019) Experimental analysis of heat transfer coefficients in phosphoric acid concentration process. J Stat Mech: Theory Exp. <https://doi.org/10.1088/1742-5468/ab2531> <https://iopscience.iop.org/article/10.1088/1742-5468/ab2531>
10. Davoudi E, Vaferi B (2018) Applying artificial neural networks for systematic estimation of degree of fouling in heat exchangers. Chem Eng Res Des 130:138–153
11. Rahimi M, Hajialyani M, Beigzadeh R, Alsairafi AA (2015) Application of artificial neural networks and genetic algorithm approaches for prediction of flow characteristic in serpentine microchannels. Chem Eng Res Des 98:147–156
12. Weber C, Tremeac B, Marvillet C, Castelain C (2016) Analysis of different fouling predictive models in a heat exchanger from experimental data. Proceedings of ECOS 2016 – The 29th International Conference on Efficiency, Cost, Optimization, simulation and environmental impact of energy systems, Portoroz, Slovenia. <https://greth.fr/analysis-of-different-fouling-predictive-models-in-a-heat-exchanger-from-experimental-data/>
13. Babuska I, Silva RS, Actor J (2018) Break-off model for CaCO_3 fouling in heat exchangers. Int J Heat Mass Transf 116:104–114
14. Behbahani RM, Muller-Steinhagen H, Jamialahmadi M (2003) Heat exchanger fouling in phosphoric acid evaporators - evaluation of field data-. In: Proc. ECI Conf. Heat exchanger fouling and cleaning: fundamentals and applications. Mexique, Santa Fé

15. Direct industry API Heat Transfer, www.directindustry.fr/prod/api-schmidt-bretten/product-39767-1872722.html (2017) (accessed 15 Mai 2017)
16. Quora. Chemical Engineering: How and why is graphite being used in heat exchangers or heating elements?, <https://www.quora.com/Chemical-Engineering-How-and-why-is-graphite-being-used-in-heat-exchangers-or-heating-elements;2017>. Accessed 15 May 2017
17. Henrotte J (2018) Turbines Hydrauliques, Pompes Et Ventilateurs Centrifuges: Principes Théoriques, Dispositions Pratiques Et Calcul Des Dimensions. Wentworth Press, France
18. Yunus AC (2007) Heat transfer: a practical approach, McGraw-Hill, pp 149. <https://www.amazon.com/Heat-Transfer-Practical-Yunus-Cengel/dp/0072458933>
19. Li W, Zhou K, Manglik RM, Li G-Q, Bergles AE (2016) Investigation of CaCO₃ fouling in plate heat exchangers. Heat Mass Transfer 52:2401–2414. <https://doi.org/10.1007/s00231-016-1752-2>
20. Demirskiy OV, Kapustenko PO, Arsenyeva OP, Matsegora OI, Pugach YA (2018) Prediction of fouling tendency in PHE by data of on-site monitoring. Case study at sugar factory. Appl Thermal Eng 128:1074–1081
21. Lee E, Jeon J, Kang H, Kim Y (2014) Thermal resistance in corrugated plate heat exchangers under crystallization fouling of calcium sulfate (CaSO₄). Int J Heat Mass Transf 78:908–916
22. Davoudi E, Vaferi B (2018) Applying artificial neural networks for systematic estimation of degree of fouling in heat exchangers. Chemical Engineering Research and Design 130:138–153
23. Wang F-L, Tang S-Z, He Y-L, Kulacki FA, Yu Y (2019) Heat transfer and fouling performance of finned tube heat exchangers : Experimentation via on line monitoring. Fuel 236:949–959
24. Fguiri A, Daouas N, Radhouani M-S, Aissia HB (2013) Inverse analysis for determination of heat transfer coefficient. Canadian J Phys 91:1034–1043

Publisher's note Springer Nature remains neutral with regard to jurisdictional claims in published maps and institutional affiliations.